Environmental Science
Water Research & Technology

ROYAL SOCIETY OF CHEMISTRY

PAPER

View Article Online
View Journal

Open Access Article. Published on 09 March 2026. Downloaded on 3/31/2026 12:53:00 PM.
This article is licensed under a Creative Commons Attribution-NonCommercial 3.0 Unported Licence.

Check for updates

Cite this: DOI: 10.1039/d5ew01138h

Nutrients recovery from wastewater using integrated vacuum and direct contact membrane distillation

A. Tahir,[a] S. Abdelsalam,[ab] S. S. Mathew,[a] H. G. Gomaa *[a] and M. B. Ray *[a]

Received 18th November 2025,
Accepted 26th February 2026

DOI: 10.1039/d5ew01138h

rsc.li/es-water

Recovery of valuable nutrients such as phosphorus from waste streams is becoming increasingly important due to the limited and constantly depleting resources and increasing consumption. In this research, the potential of using enhanced membrane distillation (MD) system for producing phosphate-rich concentrate and ammonia-water permeate from waste streams is investigated for use in different agricultural and industrial applications. MD is a promising thermally driven technology that can utilize waste and low-quality heat sources as separation driving force. The proposed system involves in-series batch recycle coupling of a direct contact membrane distillation (DCMD) and vacuum membrane distillation (VMD). The investigation included different coupling configurations as well as both synthetic and real wastewater. Results showed better performance of the coupled system compared to individual units, and that the configuration of the integrated system was important. Dimensionless sensitivity analysis revealed that permeate flux is predominantly governed by feed temperature, followed by flow rate, pH, and concentration, with temperature elasticities an order of magnitude higher than the others. Results of the analytical modeling of the coupling effect using an approximate approach were consistent with the experimental data of this work as well as with data from the literature. An order of magnitude assessment of the specific energy requirement based on using waste and low-cost heat showed that the proposed integrated MD system can be significantly more energy efficient than nanofiltration (NF) for achieving the same phosphate concentration factor (CF).

Water impact

We show that integrating vacuum and direct-contact membrane distillation enables efficient concentration of phosphorus and recovery of ammonia from real digestate using low-temperature heat sources. This offers a practical alternative to chemical precipitation or pressure-driven membranes. With validation at larger scale, the system could provide utilities with an energy-efficient route for nutrient recovery and struvite production.

1. Introduction

Fast growth in the world economy and consumption has led to a significant increase in waste generation and depletion of natural resources. This made it necessary to develop strategies and technologies to address such issues through not only waste treatment, but also recovery of valuable materials from such waste streams. Among the important nutrients that typically exist in municipal wastewater and livestock operations are nitrogen (N), and phosphorus (P).[1] The latter in particular is one of the essential nutrients for the sustenance of life that is obtained mainly from phosphorus rock, which is depleting rapidly due to the increase in demand for fertiliser.[2,3] On the other hand, the soil absorption efficiency of the used phosphorus-based fertilizer is ~15–20%, with the vast majority wasted into runoff and waste streams, leading to detrimental eutrophication of aquatic systems. One way of addressing these issues is to recover phosphate from waste streams, which not only would reduce the negative impacts of its excessive emission to the environment but also contribute to its sustainable supply in a circular economy.[4]

Different methods are available for phosphate recovery from waste streams, including chemical or biological approaches, where a sludge is formed that can be used as fertilizer. These methods, however, suffer from many drawbacks, including high cost and contamination by heavy metals, pathogens, and toxic organic compounds.[5] An alternative approach is to recover phosphate directly from the wastewater through struvite precipitation ($MgNH_4PO_4 \cdot 6H_2O$) with adequate ammonia concentration in the waste stream

[a] Chemical and Biochemical Engineering Department, Western University London, ON, N6A 5B9, Canada. E-mail: hgomaa@uwo.ca, mbhowmic@uwo.ca
[b] Department of Chemistry, Faculty of Science, Suez University, 43518 Suez, Egypt

Open Access Article. Published on 09 March 2026. Downloaded on 3/31/2026 12:53:00 PM.
This article is licensed under a Creative Commons Attribution-NonCommercial 3.0 Unported Licence.

and the external addition of magnesium (Mg) source. The efficiency of this method was found to depend significantly on the phosphate concentration in the waste streams, which is typically low for most effluents, and a concentration step may be required to enhance the process productivity and economic viability.[6–8]

Among the methods to achieve this are membrane technologies such as reverse osmosis (RO), nanofiltration (NF), and membrane distillation (MD). The latter is a thermally driven process in which molecules of volatile components traverse through the pores of a hydrophobic membrane from the feed side and condense on the permeate side, driven by the difference in vapour pressure on both sides of the pores. The technology has gained more interest recently due to many advantages, such as the potential of achieving a near 100% rejection of dissolved solids, high water permeate quality combined with low fouling potential, lower operating temperature compared to multi-stage flash and multi-effect distillation and lower operating pressure compared to RO and NF, as well as lower heat loss due to the low feed temperature. Another advantage of MD is that it can utilize low-grade heat from renewable energy such as solar and geothermal energy sources as well as heat from waste streams with temperatures close to ~50 °C or above, which further enhances the process energy efficiency and competitiveness.[9,10] Although several membrane distillation (MD) configurations have been developed, including direct contact membrane distillation (DCMD), air gap membrane distillation (AGMD), and vacuum membrane distillation (VMD), DCMD and AGMD have been most extensively studied for desalination applications,[11,12] whereas VMD has been primarily applied in cases where enhanced vapour transport or reduced permeate-side resistance is required.[13] Despite the advantages of the technology, MD has relatively low water recovery per pass, necessitating feed recirculation and/or multi-staging configuration to achieve acceptable productivity.[14,15] Research has shown that batch operation with feed recirculation has the highest energy efficiency for a given flux compared to a semibatch and continuous operation, and that multi-stage operation with feed recirculation can further enhance the system heat and recovery capabilities.[16]

Integrated and multistage membrane distillation (MD) systems have been increasingly investigated as a strategy to overcome the inherently low single-pass recovery of MD, with the majority of prior studies focusing on desalination-oriented objectives such as thermal efficiency, heat recovery, and module-level performance. Both foundational and recent works have examined multi-effect or cascaded MD configurations based on DCMD, AGMD, and VMD, predominantly through modelling approaches or experiments using saline feeds.[16–18] More specifically, Criscuoli examined integrated DCMD–VMD configurations to assess thermal behaviour and productivity relative to single DCMD units,[19] however, this work remained within a desalination framework and did not consider feed chemistry or selective species recovery. In parallel, MD-based ammonia recovery studies have primarily focused on single-module systems or modified DCMD concepts employing acidic permeate streams to enhance ammonia stripping (*e.g.*, Ding *et al.*),[20] without addressing module integration, batch concentration effects, or the simultaneous management of non-volatile nutrients.

Against this background, the present study advances integrated MD research by shifting the focus from desalination and thermal optimization to nutrient-rich wastewater treatment, where feed chemistry and species volatility fundamentally govern process behaviour. By explicitly exploiting the asymmetric transport of volatile ammonia and non-volatile phosphate, this work systematically evaluates how the coupling order of DCMD and VMD influences permeate flux, nutrient concentration, and process intensification under batch-recycle operation. DCMD and VMD configurations were selected exclusively to enable direct comparison between two distinct mass-transfer regimes-direct contact-driven and vacuum-enhanced vapor transport-thereby allowing clearer isolation of transport effects without the additional resistances present in other configurations (*e.g.*, the air gap in AGMD). The resulting phosphate-enriched retentate is suitable for downstream struvite precipitation, while the ammonia-rich permeate constitutes a recoverable nitrogen stream. The study investigates the effects of key operating and design parameters, including membrane porosity, feed temperature, and system flux, and incorporates simplified modeling to evaluate coupling effects, phosphate concentration, and specific energy consumption. Through the combined use of experiments, sensitivity analysis, and modeling, this study provides mechanistic insight into how integration sequence and wastewater composition jointly control performance, thereby addressing a gap not covered in previous integrated MD or ammonia-focused MD studies.

2. Theoretical background

The transport process in membrane distillation in general involves the transfer of the volatile component molecules from the feed side of a hydrophobic membrane to the surface, followed by transport through the membrane pores driven by the difference in vapour pressure, and vapour condensation in the membrane permeate side. In general, the mass flux J_m can be expressed as[21]

$$J_m = K(P_{fm} - P_{pm}) \quad (1)$$

In which K is the membrane coefficient (kg m^{-2} s^{-1} Pa^{-1}), P_{fm} and P_{pm} are the partial pressure at the membrane surface feed and permeate sides (Pa), respectively. The latter can be taken as the applied vacuum in VMD. The partial pressure varies with the temperature at the membrane surface on the feed and permeate sides (T_{fm} and T_{pm}), which changes with the corresponding bulk temperatures (T_f and T_p), depending on the heat transfer and flow characteristics, and can be

Open Access Article. Published on 09 March 2026. Downloaded on 3/31/2026 12:53:00 PM.
This article is licensed under a Creative Commons Attribution-NonCommercial 3.0 Unported Licence.

correlated by the temperature polarization coefficient (TPC) as,

$$\mathrm{TPC} = (T_{\mathrm{fm}} - T_{\mathrm{pm}})/(T_{\mathrm{f}} - T_{\mathrm{p}}) \tag{2}$$

The interrelation between the partial pressure and temperature is governed by the Antoine equation[22]

$$P_{\mathrm{m}}(T_{\mathrm{m}}) = 133.3 \times \exp\left[A - \frac{B}{(T_{\mathrm{m}} + C)}\right] \tag{3}$$

For the temperature range ~50–65 °C, the constants A, B, and C are 8.1, 1750, and 235, respectively. The mechanism of vapor transport through the membrane pores is governed mainly by one or a combination of Knudsen diffusion, molecular diffusion, and viscous (Poiseuille) flow mechanisms. Using an electrical analogy, the resistances contributed by the first two are added in series, which is then combined in parallel with the viscous component. The latter can be discarded for DCMD since the pressure is almost equal on both sides of the membranes, and the primary mass transport mechanism may be identified depending on Knudsen number (Kn = l/d_{p}), which is the ratio of the mean free path of the transported molecule through the membrane pores (l) to the membrane pore size (d). If Kn > 1, Knudsen diffusion is dominant, while molecular diffusion is dominant if Kn < 0.01, and the Knudsen-molecular transition occurs when 0.01 < Kn < 1. In VMD, molecular diffusion is usually neglected due to the applied vacuum and the removal of molecules from the membrane pores. Accordingly, the mass transfer is governed by Knudsen diffusion and viscous flow mechanisms. For both VMD and DCMD, an additional resistance is also added in series to account for membrane fouling, R_{f} (s m^{-1}). Expressions for the membrane distillation transport coefficient, K, may be written as,

$$K_{\mathrm{DC}} = \left[\frac{3\tau\delta}{2r\varepsilon}\sqrt{\frac{\pi RT}{8M}} + \frac{\tau\delta P_{\mathrm{a}}RT}{\varepsilon \mathrm{PDM}} + R_{\mathrm{f}}\right]^{-1} \tag{4}$$

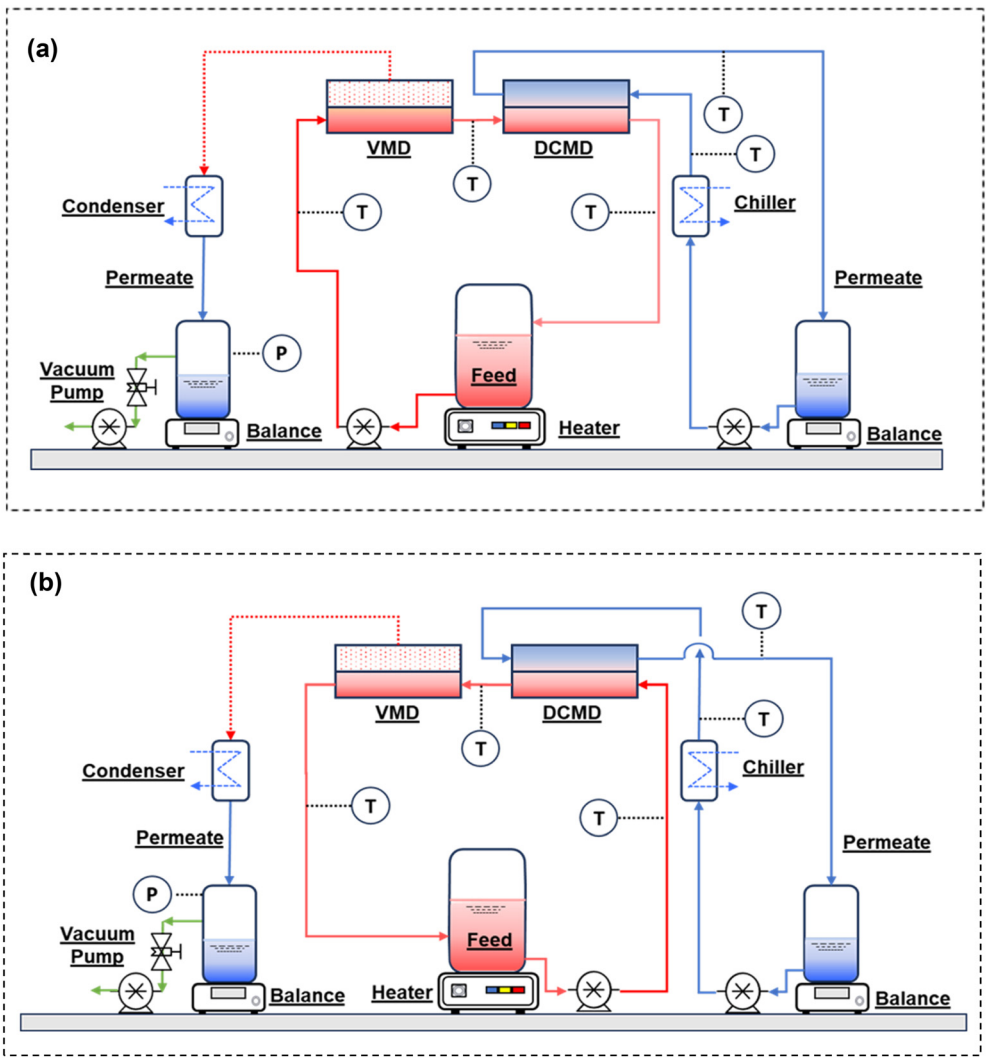

Fig. 1 Schematic for the experimental setup. a) VMD–DCMD (VD), and b) DCMD–VMD (DV).

Open Access Article. Published on 09 March 2026. Downloaded on 3/31/2026 12:53:00 PM.
This article is licensed under a Creative Commons Attribution-NonCommercial 3.0 Unported Licence.

$$K_{VM} = \left[\left(\frac{2r\varepsilon}{3\tau\delta}\sqrt{\frac{8M}{\pi RT}} + \frac{r^2\varepsilon M}{8\tau\delta\mu RT}\right)^{-1} + R_f\right]^{-1} \quad (5)$$

In the above, r is the membrane pore radius (m), ε, the membrane porosity, δ, the thickness (m), M, the molecular weight (kg kmol^{-1}), μ, the vapour viscosity (Pa s), R, the gas constant (J kmol^{-1} K^{-1}), and τ, the membrane tortuosity given by $(2-\varepsilon)^2/\varepsilon$.[23]

3. Materials and methods

Experimental set-up

The multi-staging implementation of MD investigated in this work involved in-series coupling of a VMD and a DCMD unit in batch recycle mode. The effect of the operating parameters and the coupling order of the units on the overall process permeate production was determined for two arrangements. In the first arrangement, the VMD led the DCMD and will be denoted as VD, while in the second configuration, the DCMD led the VMD and will be denoted as DV, as shown in Fig. 1a and b, respectively.

The DCMD unit was designed and fabricated in-house and was made of two bolted halves for the feed and permeate sealed by a rubber O-ring. The active area of the membrane inside the unit was 0.0047 m^2. The permeate side was cooled in a water bath using a chiller (NESLAB RTE-101) with distillate outlet temperature measured between 22–25 °C during operation. The distillate flowrate for DCMD was kept the same as the feed flowrate to minimize transmembrane pressure difference and to maintain comparable hydrodynamic conditions on both sides of the membrane interface. The VMD unit was based on SEPA membrane by Sterlitech Corporation. The active membrane area of the unit was 0.014 m^2. A vacuum pump (Fisher Scientific Maxima, model: M12C) maintained the vacuum on the permeate side. Fresh membranes were used for all experiments.

The investigation was conducted using both synthetic and real digestate wastewater solutions. The synthetic feed solution was prepared using 4.4 g of potassium phosphate (K_2HPO_4) and 22.2 g of ammonium chloride (NH_4Cl) in 3 liters of demineralized water, producing 800 mg L^{-1} of PO_4 and 2500 mg L^{-1} of NH_4. The digestate water sample was obtained from a wastewater treatment plant in London, Ontario, Canada. It was filtered through regular lab filter paper (Whatman qualitative filter paper grade 2) to remove large grit and particles that could clog the system's tubing. After filtration, the samples appeared reddish-brown and turbid, with a noticeable ammonia odor. The physical properties of the samples are shown in Table 1.

Table 1 Composition of the digestate

Component	PO_4^{3-}	NH_3	TDS	TSS	COD
Concentration (mg L^{-1})	13.2	620	1280	626	666

Membranes

The synthetic feed solution was used to conduct a preliminary thermal assessment of the membranes in the DCMD unit with laminated PTFE membranes of four different pore sizes (0.15, 0.2, 0.45, and 0.8 μm) obtained from Sterlitech Corporation. Scanning electron microscopy (SEM) was used for the membrane surface analysis (HITACHI Regulus 8230), while the membrane contact angle (CA) was measured using a goniometer (OCA-30-Germany) with 10 μL per test volume.

4. Results and discussion

4.1 Membrane characterization and screening

Thermal screening. The thermal efficiency (TE%) of the membranes was calculated using the DCMD unit[24] as,

$$\text{TE}\ (\%) = \frac{J_m A \Delta H_{v,w}}{Q_m} \times 100 \quad (6)$$

In which, J_m is the permeate flux (kg m^{-2} h^{-1}), A, membrane area (m^2), $\Delta H_{v,w}$, vaporization enthalpy (kJ kg^{-1}), Q_m, total heat flux (J) given as,

$$Q_m = m_f C_p (T_{fi} - T_{fo}) \quad (7)$$

In which m_f is the feed mass flow rate (kg s^{-1}), C_p is the feed water specific heat (kJ kg^{-1} °C^{-1}), T_{fi} and T_{fo} are the inlet and outlet feed water temperatures, respectively (°C). As can be seen in Table 2, thermal efficiency increases with the increase in the membrane pore size, mainly due to the lower hindrance to volatile compounds.

This trend reached a maximum for 0.45 μm pore size membrane, beyond which the thermal efficiency decreased with increasing membrane pore size. The decrease in efficiency could be attributed to membrane wetting, which results in membrane clogging and mass flux decay.[25] As a result, the 0.45 μm membrane was selected for use in all subsequent experiments.

Contact angle. The contact angle (CA) provides an indication of the membranes' wettability. A higher CA reflects a lower tendency of the liquid to wet the membrane surface. In general, hydrophobic solid surfaces exhibit contact angles greater than 90°. The hydrophobicity of a membrane plays a crucial role in membrane distillation (MD), as it governs surface wettability, the ability to repel the feed solution, and consequently the prevention of liquid penetration to the permeate side and mitigation of membrane fouling. The CA was measured for both pristine and used membranes. A

Table 2 Membranes thermal efficiency

Pore size (μm)	0.1	0.2	0.45	0.8
Porosity (%)	71	71	79	83
Thickness (μm)	60	40	20	20
Thermal efficiency (%)	41	62	79	60

Open Access Article. Published on 09 March 2026. Downloaded on 3/31/2026 12:53:00 PM.
This article is licensed under a Creative Commons Attribution-NonCommercial 3.0 Unported Licence.

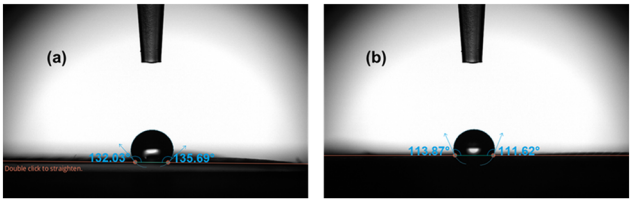

Fig. 2 Contact angle of a) pristine membrane, b) used membrane.

cumulative feed volume of 360 L was processed through the unit prior to contact angle measurements.

The results showed that most of the membrane's hydrophobicity remained intact, as shown in Fig. 2. The observed variations in CA were primarily attributed to phosphate deposition, as discussed later. This observation confirms the reliability of the experimental setup and its suitability for subsequent MD investigations.

4.2 System performance using synthetic wastewater

4.2.1 Single system MD. Mass flux was measured over a period of one hour for both DCMD and VMD configurations separately using a 0.45 μm PTFE membrane under identical operating conditions. The measured mass flux for the VMD was ~22 kg m^{-2} h^{-1} compared to ~17 kg m^{-2} h^{-1} for DCMD, indicating the higher efficiency of VMD. These results are consistent with the ranges reported by previous investigators, as shown in Fig. 3, which compares the flux values obtained in this work with the literature data.[26] The superior performance of VMD is attributed to reduced conductive heat losses and the higher transmembrane driving force arising from vacuum application on the permeate side. Moreover,

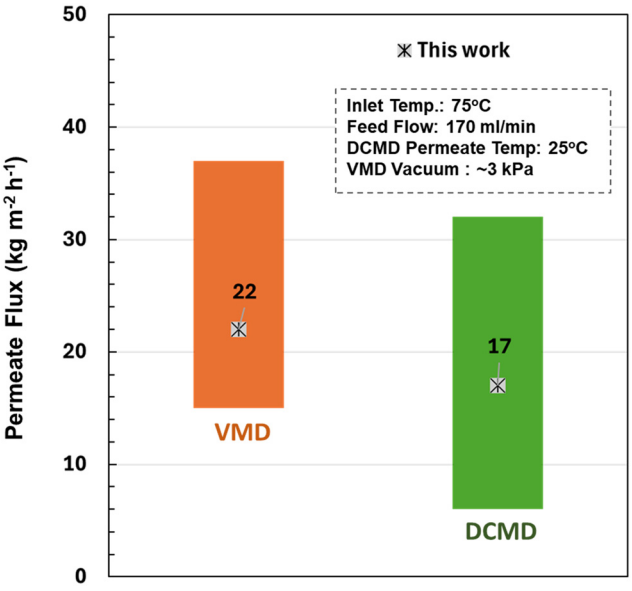

Fig. 3 Permeate mass flux in this work compared to range of data from literature.

VMD has been reported to experience lower thermal polarization, further enhancing mass transfer.[27]

Membrane fouling. The membrane surfaces of both pristine and used samples after 36 hours of operation in DCMD were examined by scanning electron microscopy (SEM) to assess the extent of surface blockage. As shown in Fig. 4, foreign particles can be seen deposited on the used membrane surface. Elemental analysis was conducted using energy-dispersive X-ray spectroscopy (EDS) (Fig. S1), which confirmed phosphorus deposition (indicated in pink in Fig. 4c). Using the mass flux and eqn (4), the fouling resistance R_f was estimated as ~1.5×10^6 s m^{-1}.

4.2.2 Integrated system performance. The influence of operating parameters on membrane distillation (MD) performance has been extensively studied for individual, uncoupled units.[28–30] These parameters, feed temperature, concentration, flow rate, pH, vacuum pressure difference (ΔP) for VMD, and cooling temperature for DCMD, similarly affect the overall performance of both units when operated in coupled configurations. Among these, feed temperature, flow rate, pH, and concentration influence both units collectively, whereas ΔP and coolant temperature affect VMD and DCMD independently. This work examined the effects of the parameters influencing both units collectively for the two integrated configurations: VD and DV. All experiments were conducted for 1 hour. As shown in the following sections, the VD configuration consistently outperformed the DV arrangement in terms of net permeate production, which can be attributed to the higher efficiency and smaller temperature drop on the VMD feed side compared with the DCMD.

Effect of feed temperature. The feed solution temperature was varied from 44 °C to 76 °C to evaluate the impact on mass flux through both configurations while all other parameters were kept constant. As shown in Fig. 5, the mass flux increased with temperature for both systems, consistent with the exponential dependence of vapor pressure on temperature in MD. VD coupling achieved a higher mass flux (~34 kg m^{-2} h^{-1} at 75 °C feed temperature) compared to the DV configuration (~24 kg m^{-2} h^{-1} at the same temperature). This enhancement can be attributed to the lower conductive losses in the VMD system,[26,31] which reduces the thermal demand on the subsequent DCMD unit. This allows higher effective vapor pressure gradients while minimizing temperature polarization and aiding in better thermal driving force utilization in the VD configuration. The observed performance difference between the two systems confirms that the coupling configuration significantly influences the overall efficiency of multistage MD systems, aligning with the simulation results previously reported.[19]

As summarized in Table 3, the variation of permeate flux with feed temperature for both VD and DV configurations was well represented by an exponential model, exhibiting strong correlations ($R^2 > 0.9$). The fitted coefficients (a and b) presented in the table indicate that flux increases markedly with temperature, confirming the strong thermal

Open Access Article. Published on 09 March 2026. Downloaded on 3/31/2026 12:53:00 PM.
This article is licensed under a Creative Commons Attribution-NonCommercial 3.0 Unported Licence.

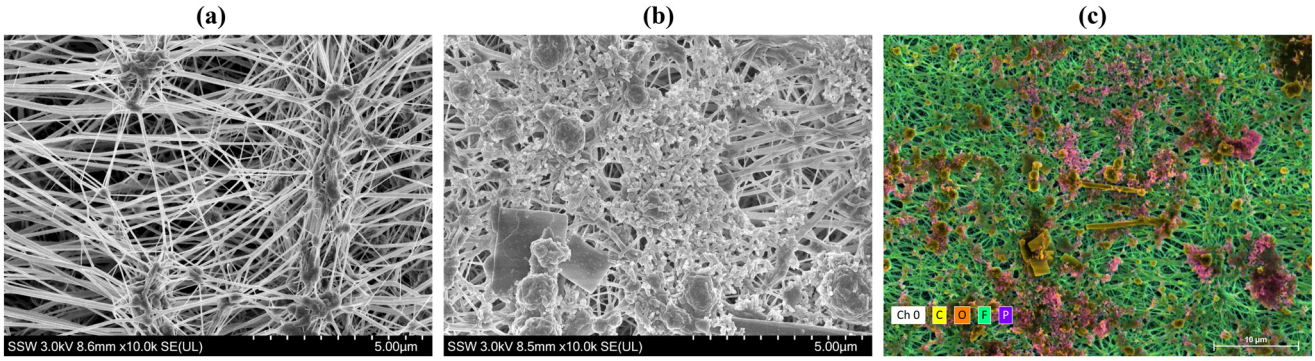

Fig. 4 SEM images of a) pristine membrane, b) used membrane, c) EDS of elemental analysis.

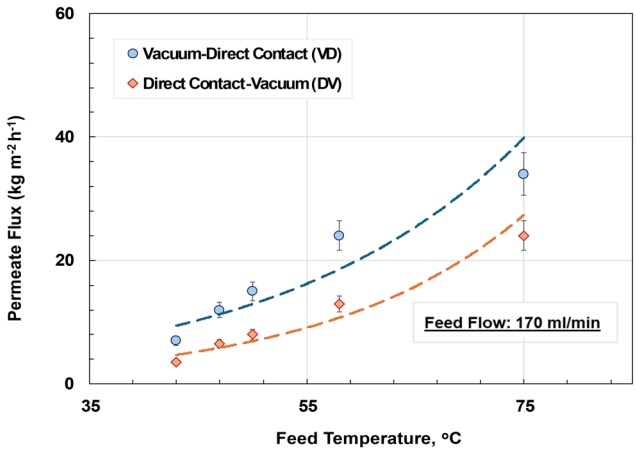

Fig. 5 Effect of feed temperature on integrated system permeate flux.

sensitivity of the process. This exponential trend arises from the temperature dependence of the vapor-pressure driving force across the membrane. In membrane distillation, flux (J) is proportional to the vapor-pressure difference between the feed and permeate sides, expressed as $J = B(P_{v,f} - P_{v,p})$, where vapor pressure P_v increases exponentially with temperature according to the Clausius–Clapeyron relation. This dependence is analogous to an Arrhenius-type expression, $J = J_0 \exp(-E_{app}/RT)$. Comparing the fitted exponential flux-temperature relationship in Table 3, with the model form allows the empirical coefficient (b) to be interpreted as an apparent activation-type energy *via* the equation, $E_{app} = bRT^2$. The estimated E_{app} values were approximately 31 kJ mol^{-1} for VD and 40 kJ mol^{-1} for DV, both within the range typically reported for MD systems.[18,32,33] The lower E_{app} for the VD configuration suggests more efficient thermal utilization, consistent with reduced conductive heat losses and a stronger vapor-phase driving force under vacuum operation.

Effect of feed flowrate. As shown in Fig. 6, the feed flow rate was varied between 80 and 250 mL min^{-1} to assess its influence on flux under otherwise identical operating conditions. Flux increased consistently with increasing flow rate for both configurations, aligning with the well-established hydrodynamic enhancement of mass transfer in membrane distillation.[34] The fitted power-law model (Table 3) described the data well ($R^2 \approx 0.99$), yielding flow exponents of 0.27 for VD and 0.21 for DV. The exponent b quantifies the elasticity of flux with respect to flow rate, indicating that a 10% increase in flow results in an approximately 2–3% rise in flux. These confirm that increasing feed velocity enhances convective heat and mass transfer, thereby reducing temperature polarization and strengthening the effective vapor-pressure driving force across the membrane.

The slightly higher flow sensitivity observed for the VD configuration suggests that the vacuum-first arrangement benefits more from hydrodynamic improvements, as reduced feed-side polarization

Table 3 Empirical flux models and fitted coefficients for temperature, flow rate, pH, and feed concentration effects in VD and DV configurations

		VD configuration		DV configuration	
Operating parameter	Fitted model	Fitted parameters	R^2	Fitted parameters	R^2
Feed temperature, T	$J = a\exp(bT)$	$a = 17.34$ $b = 0.035$	0.92	$a = 9.76$ $b = 0.045$	0.98
Feed flow rate, Q	$J = aQ^b$	$a = 8.11$ $b = 0.27$	0.99	$a = 10.05$ $b = 0.21$	0.99
Feed initial pH	$J = a(\mathrm{pH})^2 + b(\mathrm{pH}) + c$	$a = -1.27$ $b = 16.21$ $c = -18.4$	0.83	$a = -1.14$ $b = 14.51$ $c = -18.3$	0.81
Feed initial concentration, C	$J = a(C)^2 + b(C) + c$	$a = -7.4 \times 10^{-5}$ $b = 0.062$ $c = 22.14$	0.99	$a = -5.2 \times 10^{-5}$ $b = 0.041$ $c = 21.83$	0.97

Open Access Article. Published on 09 March 2026. Downloaded on 3/31/2026 12:53:00 PM.
This article is licensed under a Creative Commons Attribution-NonCommercial 3.0 Unported Licence.

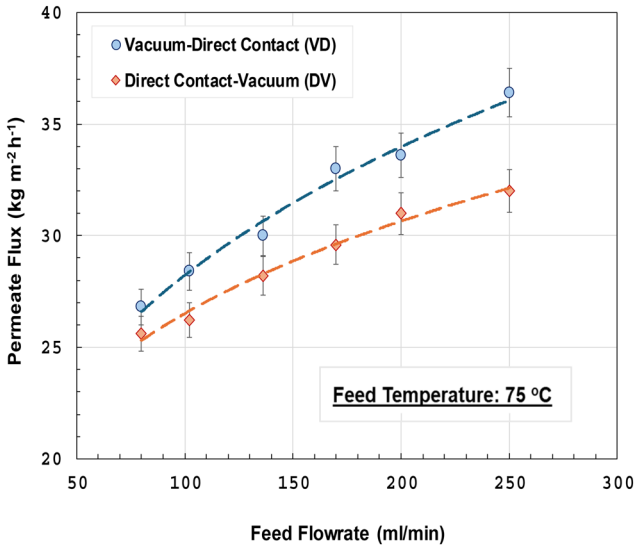

Fig. 6 Effect of feed flowrate on integrated system permeate flux.

complements its inherently lower conductive heat losses. At higher flow rates, the flux tends toward an asymptotic limit, consistent with the transition from a laminar-dominated to a fully developed flow regime, where further boundary-layer thinning provides diminishing benefit.[35,36] Overall, the power-law dependence of flux on flow rate highlights the positive hydrodynamic contribution to MD performance, while the stronger response of the VD module reflects the synergistic effect of convective enhancement and minimized heat loss under vacuum operation.

Effect of feed solution pH. The two forms of ammonia nitrogen in water are non-volatile ionic ammonium nitrogen (NH_4^+) and volatile un-ionized ammonia nitrogen (NH_3). The equilibria of these species can be expressed by the following:

$$NH_3 + H_2O \leftrightarrow NH_4^+ + OH^-$$

An increase in feed solution pH would enhance ammonia recovery on the permeate side due to an equilibrium shift towards volatile molecular NH_3 and increased transfer across the membrane. Conversely, at lower pH values, ammonia predominantly exists as the non-volatile NH_4^+ ion, which cannot be transported through non-wetted membrane pores, leading to reduced ammonia transfer. Beyond speciation and volatility effects, pH-dependant interfacial interactions at the PTFE membrane surface may also affect local ion distributions near pore entrances, providing additional explanation for the observed ammonium rejection under acidic conditions.[37,38] The effect of varying the feed pH on the membrane flux is presented in Fig. 7. The flux exhibits a parabolic dependence on pH between 2.0 and 10.0, with quadratic regression providing a good fit ($R^2 > 0.8$; Table 3). This kind of behaviour highlights the competing effects of ammonia speciation and membrane stability on MD performance. The observed increase in flux with alkalinity as the pH approaches 8.0 suggests that the partial pressure of volatile ammonia contributes synergistically to the total vapor driving force. This effect may be further enhanced by partial pore enlargement under alkaline conditions, as previously reported by Cancino-Madariaga *et al.* and Mänttäri *et al.*[39,40] However, a decline in flux was observed at pH values higher than ~8.0, caused by membrane clogging, accompanied by reduced feed clarity, likely due to scale formation that leads to partial pore blockage – an effect also noted in earlier studies on ammonia recovery by MD.[38] Overall, the VD configuration exhibited superior performance, achieving a maximum flux of ~36 kg m^{-2} h^{-1} at pH 8.0, compared to about 30 kg m^{-2} h^{-1} for the DV configurations.

Effect of feed concentration. The change in permeate flux with feed concentration was studied by changing the salt concentrations from 100 ppm PO_4^{3-} and 800 ppm NH_4^+ to 800 ppm PO_4^{3-} and 2500 ppm of NH_4^+. The results presented

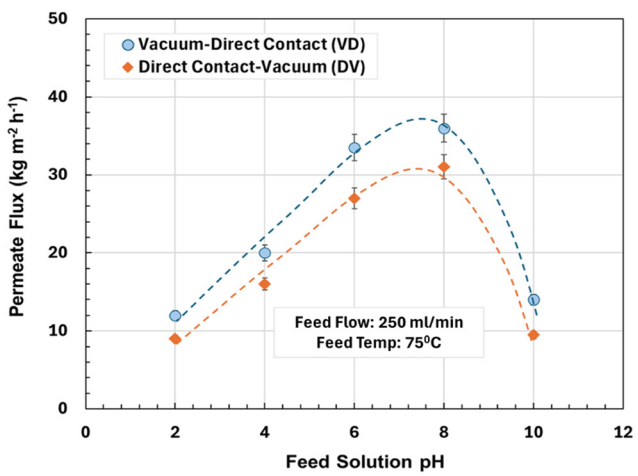

Fig. 7 Effect of feed pH on integrated system permeate flux.

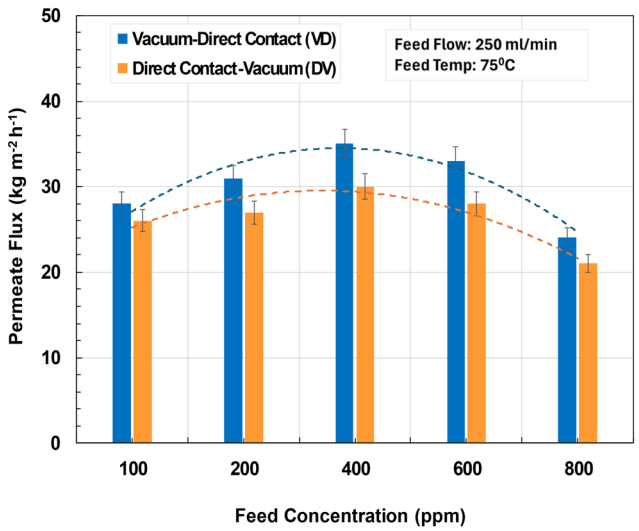

Fig. 8 Effect of feed concentration on the integrated system permeate flux.

Open Access Article. Published on 09 March 2026. Downloaded on 3/31/2026 12:53:00 PM.
This article is licensed under a Creative Commons Attribution-NonCommercial 3.0 Unported Licence.

in Fig. 8 show that the flux initially increased with phosphate concentration, reached a maximum, and then declined as concentration continued to rise. The trend is well described by a quadratic model (Table 3), with excellent fits for both configurations (R^2 = 0.97–0.99). The corresponding maximum fluxes observed at the optimum concentrations for VD and DV are 35.1 and 29.9 kg m^{-2} h^{-1}, respectively.

The initial increase in flux may be attributed to the concurrent rise in feed pH (from ~7.1 to ~8.0), which, as discussed earlier, enhances NH_3 volatility and has a positive effect on membrane flux. The subsequent decline at higher concentrations can be attributed to increased concentration polarization. As solute concentration near the membrane surface rises, the local water activity and vapor pressure decrease, thereby reducing the driving force for vapor transport across the membrane.[41,42] Precipitation of phosphate salts may also occur, resulting in partial blockage of the membrane pores. This behavior was consistent for both coupling configurations, with the VD system once again exhibiting higher fluxes and a broader optimal range than the DV configuration.

Factor influence and sensitivity analysis. To assess the relative importance of the investigated operating parameters, the results from the four parametric studies (feed temperature, flow rate, pH, and concentration) were quantitatively evaluated in terms of their dimensionless sensitivities, or elasticities (Table 4). The elasticity of flux with respect to a variable (X_i) is defined as:[43]

$$S_i = \frac{\partial J}{\partial X_i} \times \frac{X_i}{J} \tag{8}$$

Here, S_i represents the proportional change in flux (J) in response to a proportional change in X_i. A value of 1 for S_i indicates a 1% increase in flux for every 1% increase in that variable. Across all conditions, temperature exhibited the highest elasticity, indicating that flux is predominantly governed by vapor pressure gradients. The mean temperature elasticities were approximately 2.3 for the VD configuration and 2.8 for the DV configuration, implying that a 10% increase in feed temperature results in a 23–28% increase in flux. Flow rate effects were moderate (elasticities 0.21–0.27), reflecting the influence of hydrodynamic thinning of boundary layers and reduction in temperature polarization. The influence of pH was smaller but consistent (elasticities ~0.18), capturing the chemical equilibrium shift between ammonia and ammonium species and its impact on vapor-phase transport. Feed concentration showed near-zero or slightly negative elasticity values at the studied range, consistent with the opposing effects of mild pH increase and concentration polarization.

The hierarchy of parameter importance, as highlighted by the scale-independent sensitivity or elasticity value, follows the order: temperature ≫ flow rate > pH > concentration. This dominance of temperature underscores the central role of heat-driven vapor pressure gradients in governing permeate flux in the integrated MD system. The VD configuration exhibited slightly higher sensitivity to flow rate, indicating stronger hydrodynamic enhancement due to vacuum-driven mass transfer and reduced conductive losses, while the DV configuration displayed greater temperature dependence owing to the leading DCMD stage, where conductive heat losses reduce the thermal driving force available to the downstream VMD module. These observations align with the mechanistic interpretation of the sequence-dependent system performance, where configurations that preserve higher feed-side temperatures at the membrane interface achieve superior flux, while fluid dynamics and solution chemistry act as modifying influences through their effects on boundary layer development, ammonia volatility, and salt scaling.

Modeling of combined configurations. As shown before, the VD configuration always outperformed the DV arrangement in terms of permeate production under the same operating conditions. In the following section, an approximate analysis of the relative productivities of both setups is estimated, and the results are presented in terms of productivity size ratio (PS) and compared to experimental data. The PS ratio is a metric introduced to compare plants in terms of the process intensification strategy for achieving higher productivity at

Table 4 Sensitivity indices (elasticities) for VD and DV configurations

Operating parameter	Elasticity	
	VD configuration	DV configuration
Feed temperature, T	2.27	2.75
Feed flow rate, Q	0.27	0.21
Feed initial pH	0.18	0.17
Feed initial concentration, C	−0.005	−0.04

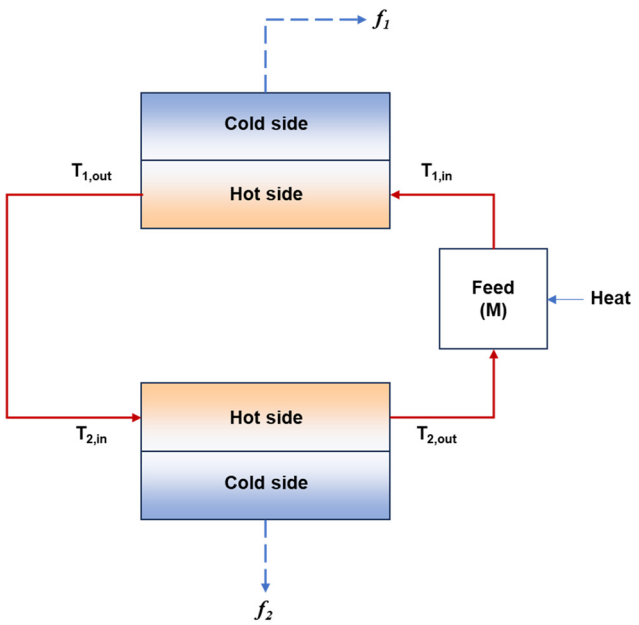

Fig. 9 Schematic of the integrated system flow model.

Open Access Article. Published on 09 March 2026. Downloaded on 3/31/2026 12:53:00 PM.
This article is licensed under a Creative Commons Attribution-NonCommercial 3.0 Unported Licence.

reduced size.[44,45] For comparing design configurations (a) and (b), the PS ratio is defined using eqn (9) as,

$$\mathrm{PS} = \frac{(\mathrm{Productivity/Size})_a}{(\mathrm{Productivity/Size})_b} \tag{9}$$

Accordingly, when the PS metric is >1, system (a) should be preferred, whereas for PS < 1, system (b) should be selected. This study assumed the same operating conditions for both configurations, and the PS ratio is estimated solely based on the permeate mass flux with no heat recovery.

In MD, the permeate flow depends on the pressure difference on both sides of the membrane, mainly dictated by the temperature on each side. In this analysis, constant vacuum and cold side temperature were assumed for the VMD and DCMD, respectively. With the aid of Fig. 9, the permeate flow was modeled in terms of the average membrane warm side temperature as,

$$f_1 \propto \eta_1 \overline{\left[T_{1,\mathrm{in}}, T_{1,\mathrm{out}}\right]} \tag{10}$$

$$f_2 \propto \eta_2 \overline{\left[T_{2,\mathrm{in}}, T_{2,\mathrm{out}}\right]} \tag{11}$$

In which η_i is a scaling efficiency taken as 0.98 for VMD and 0.40 for DCMD.[11,46] The inlet and outlet temperatures were approximately correlated using a scaling factor ξ_i as,

$$T_{i,\mathrm{out}} \cong \xi_i T_{i,\mathrm{in}} \tag{12}$$

For temperature range between 50–90 °C and using published data from the literature for feed temperature drop in VMD and DMD, values for ξ_i were found to decrease with a power of ~0.2 with an increase in the inlet temperature and ranged between ~0.98–0.88 for VMD and ~0.5–0.4 for DCMD.[17,47] Using eqn (12) in eqn (10) and (11) gives,

$$f_1 \propto \eta_1 \overline{\left[T_{1,\mathrm{in}}, \xi_1 T_{1,\mathrm{in}}\right]} \tag{13}$$

$$f_2 \propto \eta_2 \overline{\left[T_{2,\mathrm{in}}, \xi_2 T_{2,\mathrm{in}}\right]} \tag{14}$$

The total permeate output may then be expressed as,

$$f_1 + f_2 \propto \left\{ \eta_1 \overline{\left[\left\{T_{1,\mathrm{in}}, \xi_1 T_{1,\mathrm{in}}\right\}\right]} + \eta_2 \overline{\left[T_{2,\mathrm{in}}, \xi_2 T_{2,\mathrm{in}}\right]} \right\} \tag{15}$$

Since the membrane areas are the same for both systems, the PS value for the VD/DV systems can be estimated using eqn (9) as,

$$\mathrm{PS}_{(\mathrm{VD/DV})} = \frac{(f_1 + f_2)_{\mathrm{VD}}}{(f_1 + f_2)_{\mathrm{DV}}} \tag{16}$$

Eqn (16) was evaluated for alternate coupling in which VMD was leading (VD), and a reverse arrangement where DCMD is leading (DV), and taking VMD and DCMD as units 1 and 2. Fig. 10a shows the simulation results, which, as can be seen,

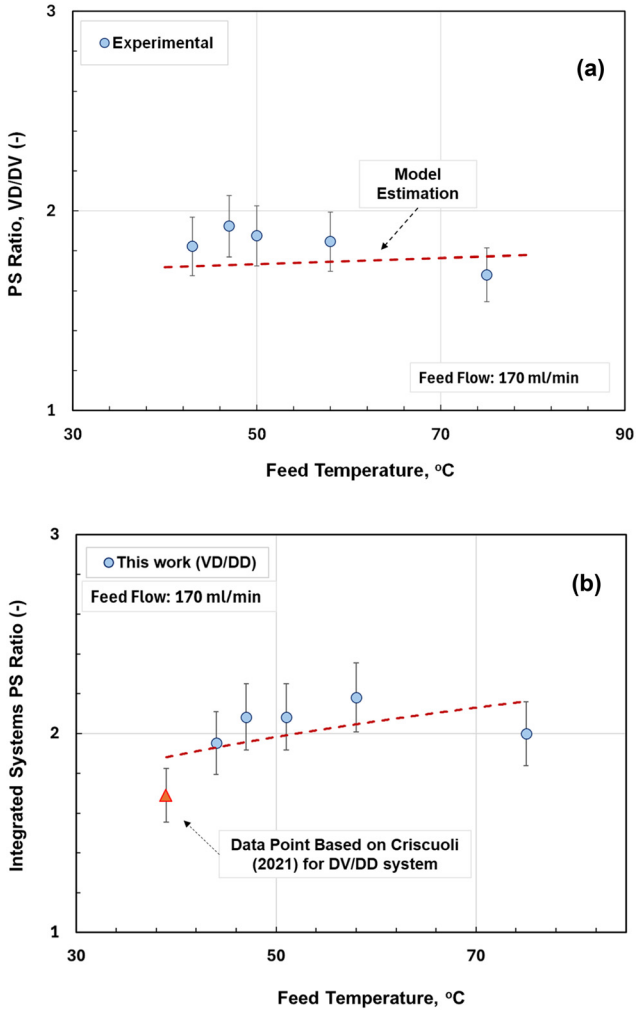

Fig. 10 MD coupling comparison (a) this work VD/DV, (b) this work VD/DD, DV/DD based on Criscuoli.[19]

reasonably agree with experimental data. Further comparison is presented in Fig. 10b between the simulated VD and two-DCMD (DD) results and the DV and DD data reported by Criscuoli[19] in which the DD integration resembled a single DCMD system.

4.3 System performance using municipal wastewater

The integrated VD system was used to treat 500 mL filtered digestate water sample obtained from a municipal wastewater treatment plant in London, Ontario, Canada. The initial feed temperature was set at 50 °C, a flow rate of 170 mL min^{-1}, and a vacuum pressure of approximately 3 kPa on the VMD permeate side. The distillate flowrate and temperature in the DCMD unit were maintained at 170 mL min^{-1} and approximately 25 °C respectively. The system operated at the natural feed pH of ~8.2 for 4.5 hours. At the end of the experiment, the phosphate concentration in the feed increased from an initial value of ~13 mg L^{-1} to ~35 mg L^{-1}, representing nearly a three-fold enrichment. No

Open Access Article. Published on 09 March 2026. Downloaded on 3/31/2026 12:53:00 PM.
This article is licensed under a Creative Commons Attribution-NonCommercial 3.0 Unported Licence.

detectable phosphate was observed in the permeate from either the DCMD or VMD units, confirming complete phosphate rejection by the membranes. The final ammonia concentration in the feed solution was ~860 mg L^{-1}, indicating sufficient enrichment for struvite precipitation. Nearly pure aqueous ammonia was recovered in the permeate streams, with concentrations of approximately 172 mg L^{-1} from the DCMD unit and 470 mg L^{-1} from the VMD unit. In practical applications, ammonia recovered *via* MD is typically stabilized through downstream conditioning steps such as acid absorption or scrubbing, converting it into stable ammonium salt solutions suitable for storage, transport, and reuse in fertilizers or industrial formulations. These post-treatment approaches are well-established in related gas–liquid separation processes,[48] while downstream stabilization and product formulation are considered part of subsequent process integration and are beyond the scope of the present study.

Concentration factor. As indicated earlier, the main objective of the process, besides treating the wastewater, is the generation of concentrated streams suitable for the production of value-added products such as struvite fertilizer. This section presents an analysis of the concentration of phosphate based on actual data, and the results are compared to those obtained using both synthetic and real municipal wastewater samples. Batch feed recirculation mode is applied, resulting in unsteady processes in which the distillate is continuously removed, and the mass of the remaining feed solution decreases while the P concentration increases with time. Applying the total P mass balance gives,

$$m(t)c(t) = M_o C_o \tag{17}$$

In which M_o and C_o are the initial feed mass (kg) and P concentration (g kg^{-1}), while $m(t)$ and $c(t)$ are the same at time t (h). Differentiating eqn (17) with respect to time and rearranging gives,

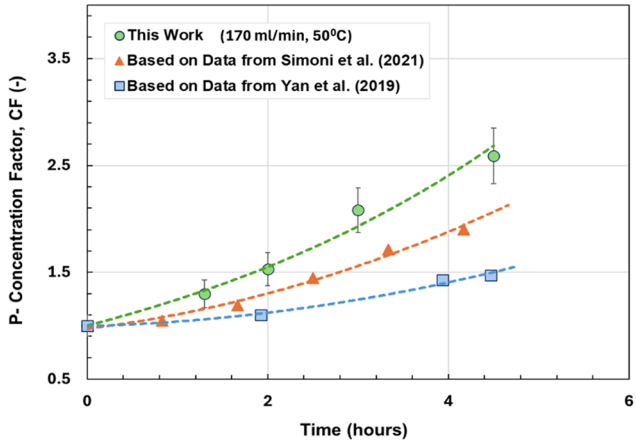

Fig. 12 Comparison of phosphate concentration change with time.[49,50]

$$\frac{dc(t)}{dt} = -M_o C_o \left(\frac{1}{m(t)^2} \frac{dm(t)}{dt} \right) \tag{18}$$

The P concentration changes from C_o to C_f within a cycle time τ_c, integrating,

$$\int_{C_o}^{C_f} dc(t) = -M_o C_o \int_0^{\tau_c} \left(\frac{1}{m(t)^2} \frac{dm(t)}{dt} \right) dt \tag{19}$$

Defining CF as the P concentration factor gives,

$$CF = \frac{C_f}{C_o} = 1 - M_o \int_0^{\tau_c} \left(\frac{1}{m(t)^2} \frac{dm(t)}{dt} \right) dt \tag{20}$$

Eqn (20) is numerically integrated by plugging values of $m(t)$ and dm/dt to evaluate the CF for the productive cycle time of the batch process, τ_c. The results in Fig. 11 show close agreement with the data obtained from experiments using both synthetic and real municipal wastewater samples. Fig. 12 presents further comparison between the results obtained in this study and examples based on data from the

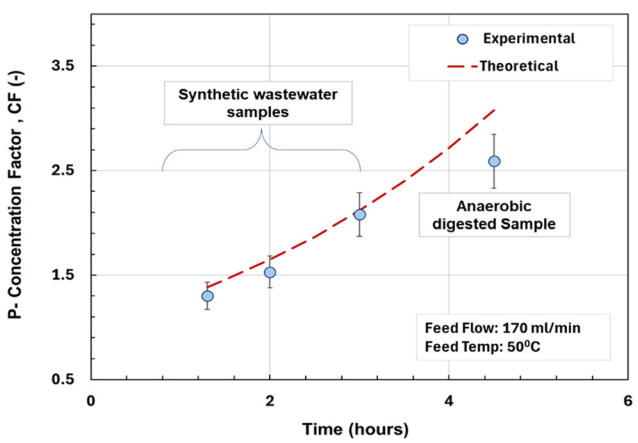

Fig. 11 Change in phosphate concentration with time.

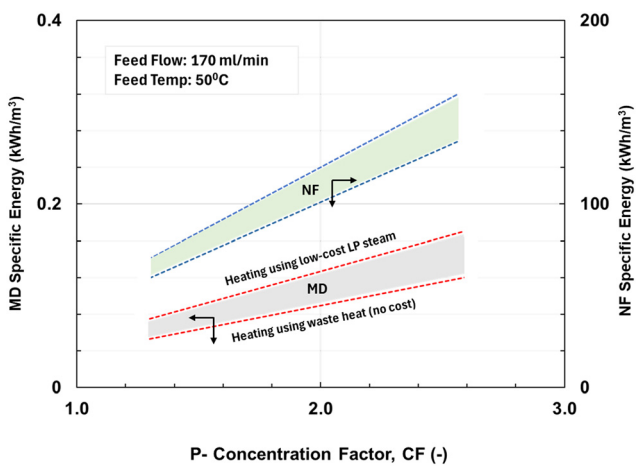

Fig. 13 Effect of phosphate CF on the specific energy consumption.

Open Access Article. Published on 09 March 2026. Downloaded on 3/31/2026 12:53:00 PM.
This article is licensed under a Creative Commons Attribution-NonCommercial 3.0 Unported Licence.

literature for investigations of P recovery from wastewater using non-integrated MD systems.[49,50]

Energy consideration. In this section, an order-of-magnitude assessment of the specific energy requirement based on the integrated system is presented. The main components of the energy cost in MD are contributed by the electrical pumping energy, which varies depending on the industrial cost of electricity, and the thermal energy required to heat the feed solution, which may not be obvious since it is typically provided by either waste heat from effluents or from low-pressure steam lines.[51] For a batch system mass of M_o (kg) circulating at a flow rate q_m (kg s^{-1}), the specific electrical pumping energy φ (kW h m^{-3}) can be estimated using,

$$\varphi = \left(\frac{10^{-6}}{3.6}\right)\frac{q_m \Delta P_s \tau_c}{M_o \eta} \tag{21}$$

In which, ΔP_s is the total pressure drop across the system (Pa), τ_c is the processing time (s), and η is the efficiency of the circulating pump (0.8).

Fig. 13 shows a representation of the effect of the P concentration factor on the specific energy estimated for a case where heating energy is provided using a waste heat source (lower limit) as well as using a low-cost (~10%) LP steam.[51] The vacuum pump energy consumption is assumed to be zero because the effect of non-condensable gas is negligible.[52] Fig. 13 also shows an estimate of the specific energy consumption using nanofiltration (NF) to achieve the same CF, which, as can be seen, is much higher than MD, provided that waste or low-cost energy is used in the latter.

Fouling, scaling, and practical considerations. Fouling and scaling are recognized challenges in membrane distillation, particularly when treating nutrient-rich wastewaters containing elevated concentrations of phosphate, ammonium, and associated counter-ions.[53] In the present study, evidence of inorganic fouling was identified through SEM-EDS analysis of used membranes, which revealed phosphorus-containing deposits on the membrane surface following extended operation. This observation is consistent with earlier reports describing the propensity of phosphate salts to precipitate and accumulate at the membrane–solution interface under conditions of concentration and temperature polarization.[49] The estimated fouling resistance ($R_f \sim 1.5 \times 10^6$ s m^{-1}), together with the limited reduction in membrane contact angle after processing a cumulative feed volume of approximately 360 L, indicates that fouling remained moderate and did not result in catastrophic wetting or irreversible performance degradation over the experimental timescale.

The integrated MD experiments were conducted in batch-recycle mode over short operational periods, with feed temperature and pH controlled to enhance flux while limiting excessive scaling. Under these conditions, complete phosphate rejection was maintained, and no solute breakthrough to the permeate was detected. Comparable short- to medium-term stability in phosphate- and ammonia-containing feeds has been reported in MD studies, where fouling is typically moderate, reversible, and manageable through operational control and periodic intervention.[20,53,54] In practice, scaling intensity can be further mitigated through standard measures such as pretreatment, pH adjustment, and intermittent physical or chemical cleaning. Rather than addressing long-term durability, this study demonstrates that within realistic operating windows for nutrient concentration and recovery, the proposed VMD–DCMD configuration can deliver enhanced productivity without rapid membrane failure, thereby providing a foundation for future investigations into long-term fouling behaviour, cleaning strategies and process scale-up.

5. Conclusions

This study demonstrated the potential of an integrated membrane distillation (MD) system for the simultaneous treatment and valorization of wastewater effluents through the concentration and recovery of phosphate and ammonia, key precursors for struvite fertilizer and other agricultural or industrial applications. The integrated configuration, comprising an in-series coupling of vacuum membrane distillation (VMD) and direct contact membrane distillation (DCMD), was shown to exhibit performance strongly dependent on the coupling order. The VMD–DCMD (VD) arrangement consistently outperformed the DCMD–VMD (DV) configuration, attributed to reduced conductive heat losses and a higher driving force on the vacuum side. An approximate predictive model was developed to capture the influence of coupling sequence, and its predictions were in good agreement with the experimental data and comparable to previously reported results. A preliminary assessment of energy demand indicated that, when operated with waste or low-grade heat sources, the integrated MD system requires substantially lower specific energy than nanofiltration (NF) to achieve an equivalent phosphate concentration factor. Overall, the findings highlight the promise of coupled MD systems as an efficient approach for nutrient recovery from waste streams. This work provides a foundation for technology developments aimed at process scale-up, long-term membrane stability, and integration within circular economy frameworks for sustainable wastewater management.

Conflicts of interest

The authors declare that they have no known competing financial interests or personal relationships that could have appeared to influence the work reported in this paper.

Data availability

All data supporting the findings of this study are presented within the manuscript.

Open Access Article. Published on 09 March 2026. Downloaded on 3/31/2026 12:53:00 PM.
This article is licensed under a Creative Commons Attribution-NonCommercial 3.0 Unported Licence.

Supplementary information (SI) is available and shows EDS spectrum of the fouled membrane and its elemental composition. See DOI: https://doi.org/10.1039/d5ew01138h.

Acknowledgements

This work was supported by the Natural Sciences and Engineering Research Council of Canada Grant # 2019-04117 awarded to the author Hassan Gomaa.

References

1 Y. Li, M. Wang and X. Chen, *et al.*, Multi-pollutant assessment of river pollution from livestock production worldwide, *Water Res.*, 2022, **209**, 117906, DOI: 10.1016/j.watres.2021.117906.
2 L. Shu, P. Schneider and V. Jegatheesan, *et al.*, An Economic Evaluation of Phosphorus Recovery as Struvite from Digester Supernatant, *Bioresour. Technol.*, 2006, **97**(17), 2211–2216, DOI: 10.1016/j.biortech.2005.11.005.
3 L. Reijnders, Phosphorus Resources, Their Depletion and Conservation, a Review, *Resour., Conserv. Recycl.*, 2014, **93**, 32–49, DOI: 10.1016/j.resconrec.2014.09.006.
4 J. R. Mihelcic, L. M. Fry and R. Shaw, Global potential of phosphorus recovery from human urine and feces, *Chemosphere*, 2011, **84**(6), 832–839, DOI: 10.1016/j.chemosphere.2011.02.046.
5 M. T. Vu, H. C. Duong and Q. Wang, *et al.*, Recent technological developments and challenges for phosphorus removal and recovery toward a circular economy, *Environ. Technol. Innovation*, 2023, **30**, 103114, DOI: 10.1016/j.eti.2023.103114.
6 C. A. Quist-Jensen, L. Wybrandt and H. Løkkegaard, *et al.*, Acidification and recovery of phosphorus from digested and non-digested sludge, *Water Res.*, 2018, **146**, 307–317, DOI: 10.1016/j.watres.2018.09.035.
7 A. Siciliano, C. Limonti and G. M. Curcio, *et al.*, Advances in Struvite Precipitation Technologies for Nutrients Removal and Recovery from Aqueous Waste and Wastewater, *Sustainability*, 2020, **12**(18), 7538, DOI: 10.3390/su12187538.
8 J. F. Hallas, C. L. Mackowiak and A. C. Wilkie, Mitigating rural WWTP impacts: System dynamics modeling of downstream nutrient outputs, *Sci. Total Environ.*, 2020, **744**, 140809, DOI: 10.1016/j.scitotenv.2020.140809.
9 A. E. Jansen, J. W. Assink and J. H. Hanemaaijer, *et al.*, Development and pilot testing of full-scale membrane distillation modules for deployment of waste heat, *Desalination*, 2013, **323**, 55–65, DOI: 10.1016/j.desal.2012.11.030.
10 N. Dow, S. Gray and J. de Li, *et al.*, Pilot trial of membrane distillation driven by low grade waste heat: Membrane fouling and energy assessment, *Desalination*, 2016, **391**, 30–42, DOI: 10.1016/J.DESAL.2016.01.023.
11 A. Alkhudhiri, N. Darwish and N. Hilal, Membrane distillation: A comprehensive review, *Desalination*, 2012, **287**, 2–18, DOI: 10.1016/J.DESAL.2011.08.027.
12 M. M. A. Shirazi and A. Kargari, A Review on Applications of Membrane Distillation (MD) Process for Wastewater Treatment, *J. Membr. Sci. Res.*, 2015, **1**, 101–112.
13 M. P. Do, G. Jiang and M. Sivakumar, A comprehensive review of vacuum membrane distillation: Applications, challenges, and future directions, *J. Water Process Eng.*, 2025, **78**, 108779, DOI: 10.1016/J.JWPE.2025.108779.
14 L. Francis, F. E. Ahmed and N. Hilal, Advances in Membrane Distillation Module Configurations, *Membranes*, 2022, **12**(1), 81, DOI: 10.3390/membranes12010081.
15 L. M. Camacho, L. Dumée and J. Zhang, *et al.*, Advances in membrane distillation for water desalination and purification applications, *Water*, 2013, **5**(1), 94–196, DOI: 10.3390/w5010094.
16 J. Swaminathan and J. H. Lienhard, Design and operation of membrane distillation with feed recirculation for high recovery brine concentration, *Desalination*, 2018, **445**, 51–62, DOI: 10.1016/J.DESAL.2018.07.018.
17 J. Gilron, L. Song and K. K. Sirkar, Design for Cascade of Crossflow Direct Contact Membrane Distillation, *Ind. Eng. Chem. Res.*, 2007, **46**(8), 2324–2334, DOI: 10.1021/IE060999K.
18 Z. Triki, Z. Fergani and H. Tahraoui, Modeling of heat and mass transfer in vacuum membrane distillation for seawater desalination, *Desalin. Water Treat.*, 2023, **313**, 12–25, DOI: 10.5004/dwt.2023.30083.
19 A. Criscuoli, Thermal performance of integrated direct contact and vacuum membrane distillation units, *Energies*, 2021, **14**(21), 7405, DOI: 10.3390/en14217405.
20 Z. Ding, L. Liu and Z. Li, *et al.*, Experimental study of ammonia removal from water by membrane distillation (MD): The comparison of three configurations, *J. Membr. Sci.*, 2006, **286**(1–2), 93–103, DOI: 10.1016/j.memsci.2006.09.015.
21 M. Qtaishat, T. Matsuura and B. Kruczek, *et al.*, Heat and mass transfer analysis in direct contact membrane distillation, *Desalination*, 2008, **219**(1–3), 272–292, DOI: 10.1016/J.DESAL.2007.05.019.
22 K. Tochigi, M. Yamagishi, S. Ando, H. Matsuda and K. Kurihara, Prediction of Antoine constants using a group contribution method, *Fluid Phase Equilib.*, 2010, **297**(2), 200–204, DOI: 10.1016/j.fluid.2010.05.011.
23 S. Srisurichan, R. Jiraratananon and A. G. Fane, Mass transfer mechanisms and transport resistances in direct contact membrane distillation process, *J. Membr. Sci.*, 2006, **277**(1–2), 186–194, DOI: 10.1016/J.MEMSCI.2005.10.028.
24 M. R. Elmarghany, A. H. El-Shazly and M. S. Salem, *et al.*, Thermal analysis evaluation of direct contact membrane distillation system, *Case Stud. Therm. Eng.*, 2019, **13**, 100377, DOI: 10.1016/j.csite.2018.100377.
25 M. Rezaei, D. M. Warsinger and V. J. H. Lienhard, *et al.*, Wetting phenomena in membrane distillation: Mechanisms, reversal, and prevention, *Water Res.*, 2018, **139**, 329–352, DOI: 10.1016/J.WATRES.2018.03.058.
26 M. C. Sparenberg, B. Hanot and C. Molina-Fernández, *et al.*, Experimental mass transfer comparison between vacuum

Open Access Article. Published on 09 March 2026. Downloaded on 3/31/2026 12:53:00 PM.
This article is licensed under a Creative Commons Attribution-NonCommercial 3.0 Unported Licence.

and direct contact membrane distillation for the concentration of carbonate solutions, *Sep. Purif. Technol.*, 2021, **275**, 119193, DOI: 10.1016/J.SEPPUR.2021.119193.

27 E. Drioli, A. Ali and S. Simone, *et al.*, Novel PVDF hollow fiber membranes for vacuum and direct contact membrane distillation applications, *Sep. Purif. Technol.*, 2013, **115**, 27–38, DOI: 10.1016/j.seppur.2013.04.040.

28 M. Gryta, Effectiveness of Water Desalination by Membrane Distillation Process, *Membranes*, 2012, **2**(3), 415–429, DOI: 10.3390/MEMBRANES2030415.

29 M. Matheswaran, T. O. Kwon and J. W. Kim, *et al.*, Factors affecting flux and water separation performance in air gap membrane distillation, *J. Ind. Eng. Chem.*, 2007, **13**(6), 965–970.

30 S. R. Selvi and R. Baskaran, Variation of Flux in Membrane Distillation, *APCBEE Proc.*, 2014, **9**, 97–101, DOI: 10.1016/J.APCBEE.2014.01.018.

31 E. Drioli, A. Ali and S. Simone, *et al.*, Novel PVDF hollow fiber membranes for vacuum and direct contact membrane distillation applications, *Sep. Purif. Technol.*, 2013, **115**, 27–38, DOI: 10.1016/j.seppur.2013.04.040.

32 M. O. J. Azzam, S. I. Al-Gharabli and F. F. Alrawash, Air gap membrane distillation applied to olive mill wastewater, *J. Environ. Chem. Eng.*, 2022, **10**(5), 108465, DOI: 10.1016/j.jece.2022.108465.

33 M. P. Godino, V. M. Barragán and M. A. Izquierdo, *et al.*, Study of the activation energy for transport of water and methanol through a Nafion membrane, *Chem. Eng. J.*, 2009, **152**(1), 20–25, DOI: 10.1016/j.cej.2009.03.022.

34 M. Gryta and M. Tomaszewska, Heat transport in the membrane distillation process, *J. Membr. Sci.*, 1998, **144**(1–2), 211–222, DOI: 10.1016/S0376-7388(98)00050-7.

35 M. Suleman, M. Asif and S. A. Jamal, Temperature and concentration polarization in membrane distillation: a technical review, *Desalin. Water Treat.*, 2021, **229**, 52–68, DOI: 10.5004/dwt.2021.27398.

36 H. Al-Sairfi, M. Z. A. Koshuriyan and M. Ahmed, Membrane distillation of saline feeds and produced water: A comparative study of an air-gap and vacuum-driven modules, *Desalin. Water Treat.*, 2024, **317**, 100145, DOI: 10.1016/j.dwt.2024.100145.

37 A. Barišić, J. Lützenkirchen and G. Lefévre, *et al.*, The influence of temperature on the charging of polytetrafluoroethylene surfaces in electrolyte solutions, *Colloids Surf., A*, 2019, **579**, 123616, DOI: 10.1016/j.colsurfa.2019.123616.

38 P. P. Kywe and C. Ratanatamskul, Influences of Permeate Solution and Feed pH on Enhancement of Ammonia Recovery from Wastewater by Negatively Charged PTFE Membranes in Direct Contact Membrane Distillation Operation, *ACS Omega*, 2022, **7**(31), 27722–27733, DOI: 10.1021/acsomega.2c03673.

39 B. Cancino-Madariaga, C. F. Hurtado and R. Ruby, Effect of pressure and pH in ammonium retention for nanofiltration and reverse osmosis membranes to be used in recirculation aquaculture systems (RAS), *Aquac. Eng.*, 2011, **45**(3), 103–108, DOI: 10.1016/J.AQUAENG.2011.08.002.

40 M. Mänttäri, A. Pihlajamäki and M. Nyström, Effect of pH on hydrophilicity and charge and their effect on the filtration efficiency of NF membranes at different pH, *J. Membr. Sci.*, 2006, **280**(1–2), 311–320, DOI: 10.1016/J.MEMSCI.2006.01.034.

41 M. Gryta, Concentration of NaCl solution by membrane distillation integrated with crystallization, *Sep. Sci. Technol.*, 2002, **37**(15), 3535–3558, DOI: 10.1081/SS-120014442;JOURNAL:JOURNAL:LSST19;REQUESTEDJOURNAL:JOURNAL:LSST20;WGROUP:STRING:PUBLICATION.

42 E. Jang, S. H. Nam and T. M. Hwang, *et al.*, Effect of operating parameters on temperature and concentration polarization in vacuum membrane distillation process, *Desalin. Water Treat.*, 2015, **54**(4–5), 871–880, DOI: 10.1080/19443994.2014.952673.

43 F. Banat, F. A. Al-Rub and K. Bani-Melhem, Desalination by vacuum membrane distillation: sensitivity analysis, *Sep. Purif. Technol.*, 2003, **33**(1), 75–87, DOI: 10.1016/S1383-5866(02)00221-6.

44 A. Criscuoli and E. Drioli, New Metrics for Evaluating the Performance of Membrane Operations in the Logic of Process Intensification, *Ind. Eng. Chem. Res.*, 2006, **46**(8), 2268–2271, DOI: 10.1021/IE0610952.

45 A. Stankiewicz and J. A. Moulijn, Process Intensification: Transforming Chemical Engineering, *Chem. Eng. Prog.*, 2000, **96**, 22–33.

46 S. O. Olatunji and L. M. Camacho, Heat and mass transport in modeling membrane distillation configurations: A review, *Front. Energy Res.*, 2018, **6**, 421215, DOI: 10.3389/FENRG.2018.00130/FULL.

47 R. Ullah, M. Khraisheh and R. J. Esteves, *et al.*, Energy efficiency of direct contact membrane distillation, *Desalination*, 2018, **433**, 56–67, DOI: 10.1016/J.DESAL.2018.01.025.

48 M. Farghali, Z. Chen and A. I. Osman, *et al.*, Strategies for ammonia recovery from wastewater: a review, *Environ. Chem. Lett.*, 2024, **22**(6), 2699–2751, DOI: 10.1007/S10311-024-01768-6.

49 Z. Yan, H. Yang and F. Qu, *et al.*, Application of membrane distillation to anaerobic digestion effluent treatment: Identifying culprits of membrane fouling and scaling, *Sci. Total Environ.*, 2019, **688**, 880–889, DOI: 10.1016/J.SCITOTENV.2019.06.307.

50 G. Simoni, B. S. Kirkebæk and C. A. Quist-Jensen, *et al.*, A comparison of vacuum and direct contact membrane distillation for phosphorus and ammonia recovery from wastewater, *J. Water Process Eng.*, 2021, **44**, 102350, DOI: 10.1016/J.JWPE.2021.102350.

51 A. Yadav, P. K. Labhasetwar and V. K. Shahi, Membrane distillation using low-grade energy for desalination: A review, *J. Environ. Chem. Eng.*, 2021, **9**(5), 105818, DOI: 10.1016/j.jece.2021.105818.

52 U. K. Kesieme, N. Milne and H. Aral, *et al.*, Economic analysis of desalination technologies in the context of carbon pricing, and opportunities for membrane distillation, *Desalination*, 2013, **323**, 66–74, DOI: 10.1016/J.DESAL.2013.03.033.

Open Access Article. Published on 09 March 2026. Downloaded on 3/31/2026 12:53:00 PM.
This article is licensed under a Creative Commons Attribution-NonCommercial 3.0 Unported Licence.

53 L. D. Tijing, Y. C. Woo and J. S. Choi, *et al.*, Fouling and its control in membrane distillation—A review, *J. Membr. Sci.*, 2015, **475**, 215–244, DOI: 10.1016/J.MEMSCI.2014.09.042.

54 M. Gryta, The long-term studies of osmotic membrane distillation, *Chem. Pap.*, 2017, **72**(1), 99–107, DOI: 10.1007/S11696-017-0261-1.

 This journal is © The Royal Society of Chemistry 2026